"Characteristics and stability of sensorimotor activity driven by isolated-muscle group activation in a human with tetraplegia"

Robert W. Nickl[1], Manuel A. Anaya[1], Tessy M. Thomas[2], Matthew S. Fifer[5], David P McMullen[6], Margaret C. Thompson[5], Daniel N. Candrea[2], William S. Anderson[4,] Brock A. Wester[5], Francesco V. Tenore[5], Nathan E. Crone[3], Pablo A. Celnik[1,2], Gabriela L. Cantarero[1]

1. Dept. of Physical Medicine and Rehabilitation, Johns Hopkins School of Medicine

2. Dept. of Biomedical Engineering, Johns Hopkins School of Medicine

3. Dept. of Neurology, Johns Hopkins School of Medicine

4. Dept. of Neurosurgery, Johns Hopkins School of Medicine

5. Research and Exploratory Development Department, Johns Hopkins Applied Physics Laboratory

6. National Institute of Mental Health, National Institutes of Health

* Corresponding author: Gabriela L Cantarero (gcantar1@jhmi.edu)

ABSTRACT

The topography and temporal stability of movement representations in sensorimotor cortex underlie the quality and durability of neural decoders for brain machine interface (BMI) technology. While single- and multi-unit activity (SUA and MUA) in sensorimotor cortex has been used to characterize the layout of the sensorimotor map, quantifying its stability has not been done outside of injury or targeted interventions. Here we aimed to characterize 1) the bilateral sensorimotor body map associated to isolated muscle group contractions and 2) the stability of multiunit firing responses for a single muscle (the extensor carpi radialis, ECR) over short (minutes) and long (days) time intervals. We concurrently recorded surface electromyograms (EMG) and MUA in a participant with

incomplete high-spinal-cord injury as he executed (or attempted to execute) different metronome-paced, isolated muscle group contractions. Furthermore, for 8 recording sessions over 2 months, we characterized the sensorimotor map associated to ECR motions both within and across sessions. For each measurement period, we compared the stability of somatotopy (defined by the number of the channels on which a response was consistently detected) and firing pattern stability for each responsive channel. Stability was calculated for each channel in peri-EMG or peri-cue windows using both mean MUA firing rates and the full time-varying responses (i.e., MUA “shape”). First, we found that cortical representations of isolated group muscle contractions overlapped, even for muscles from disparate body regions such as facial and distal leg muscles; this was the case for both intact and de-efferented muscles, in both motor and sensory channels. Second, the spatial stability of somatotopy significantly changed over the course of both minutes and days, with the consistency between sessions decreasing across longer bouts of time. Firing pattern stabilities showed distinct profiles; mean MUA firing rates became less stable over time whereas MUA shape remained consistent. Interestingly, sensory channels were overall more consistent than motor channels in terms of spatial stability, mean MUA firing rates, and MUA shape. Our findings suggest that the encoding of muscle-driven specific activity in sensorimotor cortex at the level of MUA is redundant and widespread with complex spatial and temporal characteristics. These findings extend our understanding of how sensorimotor cortex represents movements, which could be leveraged for the design of non-traditional BMI approaches.

INTRODUCTION

Many efforts have been made to topographically map the body onto the primary motor cortex (M1; Penfield and Boldrey 1937; Becker 1953; Leyton and Sherrington 1917; Lotze et al. 2000; Meier et al. 2008). Historically, stimulation studies indicated that individual body parts are represented with a partially-fractionated somatotopy - with the face, arm, and legs seated in largely distinct areas, whereas individual muscles within an effector are represented in a more mixed and overlapping fashion (Schieber and Hibbard, 1993; Graziano 2006). A recent study contradicted this viewpoint, providing evidence of intermixed whole-body tuning in the hand knob area of human M1 (Willett et al. 2020).

Although much work has focused on characterizing the layout of the sensorimotor map, comprehensive work to quantify its stability is lacking. Stability in the neural representation of a given movement can be conceptualized both by the consistency in location of active units and by the dynamics of their firing responses. Studies exploring sensorimotor map changes have been limited to injury and disease (such as amputation or stroke), or targeted interventions such as drugs or intense motor training (Schieber et al. 2009; Nudo and Milliken 1996; Nudo, Milliken, et al. 1996; Nudo, Wise, et al. 1996; Kleim, Barbay, and Nudo 1998; Gaser and Schlaug 2003; Franchi 2002). Additional studies have explored the stability of individual motor neurons and their tuning characteristics, though with opposing views about whether motor encoding is stable at the individual-unit level (Suner et al. 2005 Ganguly and Carmena 2009; Greenberg and Wilson 2004; Chestek et al. 2007; Fraser and Schwartz 2012), or is instead continuously evolving so that stability is only manifested at the ensemble level (Gallego et al. 2017; Carmena et al. 2005; Rokni et al. 2007; Li, Padoa-Schioppa, and Bizzi 2001). While most of this data derives from non-human primates (NHPs), results from humans have been similarly ambivalent, with some studies suggesting that single-units and multi-units (SU and MU) can be consistently identified for months, whereas others changed within a single day (Downey et al. 2018).

Interestingly, despite evidence suggesting motor units can show long-term stability, the same longevity has not been present for the performance of brain machine interfaces (BMI). Neural decoders for BMI technology rely on mapping firing rates of recorded units with actuated (or attempted) movement kinematics, and that their spatial distribution and activity patterns are consistent over time. Accordingly, one would expect that the long-term stability in the encoding of actions would translate to the longevity of performance of a trained neural decoder. Yet, while some trained neural decoders have maintained consistent performance over multiple sessions in NHPs (Ganguly and Carmena 2009), in humans they have largely failed to maintain consistent performance for more than a single session - sometimes even requiring retraining of a neural decoder within the same session (Ajiboye et al. 2017; Bouton et al. 2016; Hochberg et al. 2012; 2006; Collinger et al. 2013; Klaes et al. 2015; 2014; Downey et al. 2018), although these instabilities can be at least partially overcome with algorithmic approaches (Degenhart et al. 2020).

The goal of this study was to characterize the stability of the sensorimotor map over varying time periods, both in terms of its spatial arrangement and the firing patterns of its neurons. In this study, we tested the hypothesis that the multi-unit sensorimotor map changes over time, even in the absence of injury or interventions. Our findings provide evidence that the somatotopy and mean firing rates of MUA varies significantly as the period between consecutive measurements increases from minutes to days, with stability of sensory units being categorically higher than that of motor units. Similarly, peristimulus-time histogram (PSTH) wave shapes are more stable for sensory units than motor units, however, their consistency between consecutive measurements is not significantly affected by the passage of time.

METHODS

This study was conducted under an Investigational Device Exemption (IDE) by the FDA (G170010) and approved by the Johns Hopkins School of Medicine and NIWC Pacific Institutional Review Boards (IRBs). A C5/6 incomplete ASIA B tetraplegic male (48 years old; 31 years post injury; right hand dominant) was implanted bilaterally with six

cortical microelectrode arrays (NeuroPort; Blackrock Microsystems, Salt Lake City, UT): 4 in the dominant hemisphere (2 in M1, 2 in S1) and 2 in the nondominant (1 each in M1 and S1) (Fig. 1A). The participant has retained control of facial, head, and upper trunk muscles with residual control of bilateral shoulder abductions and wrist extensions,

Experimental Design:

Characterization of Full-Body Sensorimotor Map: To comprehensively characterize the sensorimotor map somatotopy and MUA firing patterns we asked the participant to attempt paced and repeated isolated group movements to a metronome while simultaneously recording surface electromyograms (EMG) and MUA from all sensorimotor MEAs (Figure 1B and 1C). Those movements consisted of systematically executing (or attempting) unilateral isolated group contractions from 30 intact and paralytic muscles throughout the body (Fig. 3A).

Prior to each recording, the participant was carefully situated into a posture that was both comfortable and eliminated any extraneous EMG activity outside the targeted muscle (including any postural muscles). For some muscles, the participant required training to ensure proper isolation, where he practiced movements while a trained experimenter monitored the EMG on the targeted and surrounding muscles and provided verbal feedback. Once adequate isolation was achieved, the metronome would be turned on and the concurrent recordings of EMG and MUA would begin. Recording blocks for each muscle consisted of 30 repetitions of isolated group muscle contractions at a period of 4 s (lasting approximately 2 min). Contractions were cued using paced metronome ticks, which consisted of a simultaneous auditory beep with an onscreen flash of a gray patch (durations 750 ms). A photodiode was used to mark the cue onset for referencing during offline analysis. During each recording block, one experimenter attended to the participant's EMG activity and another observed them physically to ensure compliance and proper muscle isolation. A trial was considered noncompliant and removed from analysis whenever extraneous muscle activity was detected or the participant failed to respond in time, with the exception of absent EMG from paralyzed muscles.

Characterizing Stability of ECR Sensorimotor Map: To characterize the stability of the sensorimotor map, we focused on repeated characterizations of the sensorimotor map of the extensor carpi radialis (ECR), a muscle-contraction the participant was reliably capable of performing, using the same paradigm as described above. These characterizations were repeated 2 times daily (separated by 1 min) across 8 days over the course of two months (approximately twice per week).

EMG and MUA Recordings: EMG recordings of the targeted muscle, its contralateral homologue, adjacent muscles, and select postural muscles were recorded across all trials (AMT-8; Bortec Biomedical, Calgary, AB, Canada). MUA data was auto-thresholded at the outset of each experiment, using a reference level of –3.5 dB of resting-level activity measured that day. EMG and MUA data were recorded with Blackrock Neural Signal Processors (Blackrock Microsystems, Salt Lake City, UT) and inspected online using the Central software suite (Blackrock Microsystems). EMG and photodiode channels were sampled at a rate of 2 kHz, while cortical signals from the Blackrock microarrays were sampled at 30 kHz. Experimental software and analyses were coded in MATLAB (MathWorks, Natick, MA).

Data Analysis:

Stability Metrics: We quantified the stability of the sensorimotor map (i.e. how consistent MUA responses are between measurement periods) across two timescales: minutes (across blocks) and days (across sessions). Stability was characterized as changes in somatotopy (i.e. *spatial stability*) and changes in MUA firing patterns. *Spatial stability* was defined as the consistency with which a given channel was active during contraction of a given muscle. This was quantified as the number of channels on which a response was consistently detected across blocks and days for a given muscle contraction. MUA firing pattern stability for each responsive channel was quantified across blocks and sessions using two measures: *mean MUA firing rate* (similarity of average firing rates in a response window anchored around EMG-burst/cue onsets across timescales) and *MUA shape* (similarity of the overall PSTH waveform across timescales). The similarity of MUA response patterns was calculated using the

Intraclass Correlation Coefficient (ICC), a measure of reliability across multiple measurements that ranges from 0 (little / no agreement between assessments) to 1 (maximum agreement between assessments) (Shrout and Fleiss, 1979; Birn et al., 2013). To compare *mean MUA firing rate* over time, we computed ICC for mean firing responses, where each active channel corresponded to a measurement instance (either blocks or days apart). For comparing consistency of *MUA shapes* over time, we repeated the ICC calculations, but this time considered each measurement to be the PSTH waveform. To maintain consistent sampling size across timescales, stability comparisons for day-to-day analyses were limited to averages of the first 15 trials for each block over separate days, while minute-to-minute analyses were between the first 15 and last 15 trials within a block.

EMG analysis: EMGs were processed using standard techniques (deLuca et al., 2010). Raw signals were bandpass filtered at [20, 400] Hz, and envelopes were detected using rectification in tandem with further lowpass filtering (5 Hz). All filtering was non-causal.

EMG Trial-Screening: EMG signals across all recorded muscles for each trial were visually inspected for invalid responses such as co-contractions with the targeted muscle, spasms (synchronous high-amplitude global muscle activations), or missed responses (lack of EMG response from an intact target muscle). When the subtask involved muscles below the level of injury, where EMG was expected to be absent, only the former two criteria were used as bases for trial exclusion.

EMG Burst-Onset: EMG burst onset was detected using a multistage process. First, the EMG was epoched from -1 to 2 seconds relative to each stimulus cue, where cues where presented at mean intervals slightly above 4 s (4.05 s) due to random jitter. Second, within this epoch, signals were normalized to their local peak-to-peak amplitudes and local peaks were identified. Third, response onsets and terminations were determined by calculating the nearest time points around the EMG peak where the amplitude crossed a threshold of 1.1 times the mean level within the window. This threshold was adjusted slightly higher on a per-block basis depending on the noise floor of the EMG during a given recording session.

Peristimulus-Time Histograms (PTSH): Spike times across all channels were windowed into individual trials, using brackets of -0.300 to 1 s relative to the start of either each EMG onset (for intact muscles) or the stimulus cue (for paralytic muscles without discernable EMG responses), as illustrated in Figure 2. Spiking rates were calculated by binning these spike times into peristimulus-time histograms (PSTHs) at 1 ms resolution, dividing by the bin width, and smoothing them with Gaussian kernels of 100 ms. Channel spiking data is presented as the average of smoothed PSTHs across trials with 95% bootstrapped confidence intervals.

Identification of active channels: Candidate channels for muscle-related neural activity were identified using a sliding-window method (Sugase-Miyamoto and Richmond 2005; Levakova et al. 2015). Each set of trial-referenced spike density curves was partitioned into a fixed baseline window from -250 ms to -150 ms relative to EMG burst onset (or cue onset for paralytic muscles), and a 100 ms response window that was slid in 5-ms increments starting at -150 ms prior to burst/cue onset until 1000 ms post burst / cue. For each position of the response window, the time-averaged baseline and response window over all trials were compared using two-tailed paired-t tests. Whenever the response window was significantly different from the baseline window ($p \leq 0.01$) for at least 4 consecutive windows (Sugase-Miyamoto and Richmond, 2005), the channel was flagged as statistically modulated. Note that this threshold is comparable to a widely-used technique, which typically employs a threshold of the mean firing rate plus 1-3 times the standard deviation of the baseline firing rate (Maunsell and Gibson, 1992; Churchward et al., 1997; Eifuku et al. 2004). Flagged channels were then validated by a human rater blinded to the channel and target muscle. Channels that passed both the statistical threshold and rater inspection were considered significantly activated by the task. Neural response times of each active channel were calculated by finding the earliest window delay at which the 4-consecutive-window criterion was met, and then computing the median time within that window (Sugase-Miyamoto & Richmond, 2005). The end of the response was ascribed to the median of the window where a violation of the 4-window criterion was detected (i.e. the significance level of the firing rate with respect to baseline exceeded 0.01). MUA response firing rates were calculated within

the response windows inferred from this process; in cases that the sliding-window method detected multiple response times, the mean firing rate of the longest response interval was used.

RESULTS

Muscle contractions throughout the body evoke diffuse, overlapping MUA on bilateral motor and sensory arrays

All 30 muscles groups across the whole-body survey were categorized into 7 regions (face, proximal arm, distal arm, fingers, core, proximal leg, and distal leg) (Figure 3A). The comprehensive body map of a single motor (Fig 4B, top panel) and sensory (Fig 4B, bottom panel) MEA from pedestal B is depicted with color patches indicating significantly modulated channels for a specific body region. All regions of the body were represented throughout the motor MEA (facial: 69.8% of multi-units; core: 18.8%; shoulder and elbow: 80.2%; wrist: 69.8%; fingers: 57.3%; hip and knee: 26.0%; ankle and foot: 38.5%), with nearly all channels (95.8%) in the motor MEA being active for multiple muscle regions. Though the motor array was implanted in the hand knob, we noted that activity was induced by muscle contractions (executed or attempted) from facial to distal leg regions, despite occupying laterally opposite somatotopic regions, and by tasks involving both well-controlled and paralytic muscles (100% and 52.1% of multi-units, respectively). In addition, a majority of channels (71.9%) also engaged during ipsilateral contractions. Analogous results were found on the corresponding sensory MEA, in terms of body-wide representation (facial: 84.4% of multi-units; core: 46.9%; shoulder and elbow: 81.3%; wrist and fingers: 100%; hip and knee: 43.8%; ankle and foot: 58.3%), modulation across multiple regions (100%); modulation of intact and paralyzed muscles (100% and 69.4% of units respectively), and ipsilateral contractions (90.6%). Altogether, the sensorimotor somatotopy provides evidence of a global and bilateral body representation within the hand knob and S1 representation of the hand.

Spatial stability of sensorimotor somatotopy is sensitive to the passage of time and to a greater extent in motor than sensory channels

We compared the spatial arrangement of responses over two timescales: minutes (i.e. blocks) and days. Figure 4 shows the activation maps over two consecutive blocks (Fig 4A) and over two consecutive days (Fig 4B) for a pedestal B motor (top panel) and sensory (bottom panel) MEA. First, we evaluated the extent to which muscles over each of 7 segments throughout the body were represented across the arrays. Then, as a measure of the spatial stability, we counted the number of channels active on motor and sensory arrays during recording periods separated by minutes or days, and counted the frequency of overlapping channels.

Motor Arrays: Only a small fraction of the total channels was consistently active across a given span of blocks and days; however, their locations on the arrays were similar between consecutive measurements: Figures 4A and 4C (top rows) compare, for right ECR, typical block-to-block (timescale of minutes) and session-to-session (timescale of days) the locations of active channels. In this case, the locations of active channels on motor arrays are fairly consistent between consecutive time points (within minutes or within days). On the order of minutes, 11 motor channels were active within a block, with 7 of those same 11 channels remaining active in the subsequent block (Fig 5A). On the timescale of days these numbers were higher, 16 motor channels were active with a day with 14 of those same 16 channels present both days.

Sensory Arrays: Active channels on the sensory array were more numerous than for the motor array. On the order of minutes (Fig. 4A, bottom), a total of 21 sensory channels were active, with 9 of 21 being present both minutes. Across sessions (Fig 4B, bottom), 22 channels were responsive for right wrist extensions, with 19 of 22 being active on both days.

Overall, we also found the prevalence of active channels in motor cortex was less stable than in sensory cortex. Figure 5A summarizes the spatial stability for all pedestals in terms of raw counts of responsive channels across each number of days. Here we see

a total of 17 channels across all motor arrays were active for at least 1 session with a majority of stable motor channels (10 / 17 channels = 58.8%) active for less than half of the sessions (4 or fewer). In contrast, a total of 58 channels across all sensory arrays were active for at least 1 experiment session with most responding over all 8 days (79.3%). For both motor and sensory MEAs, the number of active channels observed for all 8 sessions is fewer than the number of channels observed across a subset of 7 sessions, 6 sessions, and so forth. To contextualize the magnitude of these changes to better reflect spatial stability, we divided them by the total number of active channels observed on at least one day. A two-way ANOVA of the percentage changes reveals a significant main effect of brain region ($F_{(6,1)}=21.04, p<0.005$), but not of time ($F_{(6,1)}=2.03, p = 0.2052$). When comparing the percentage channel decline across number of days and the cortical region (i.e. motor vs sensory), we found a significantly larger decline for motor than sensory channels ($F_{(6,1)}=21.04, p<0.005$). In other words, as more days are included in the stability analysis, motor arrays show a proportionally larger decline in the number of consistently active channels than do sensory channels. This implies that sensory channels were more stable over time than motor channels.

MUA firing rates are sensitive to passage of time and to a greater extent in motor than sensory channels

We compared the mean MUA firing rate of active channels along a timescale of minutes (i.e. blocks) and days. Using a heat map where warmer colors denote higher firing rates, Figure 4 illustrates the intensity of each channel's trial-averaged firing rate over two consecutive blocks (Fig 4A) or two consecutive days (Fig 4 C). Figures 5B and 5C show the distribution of ICCs of average MUA firing rates for each brain region across each time scale. Using a two-way repeated measures ANOVA to compare the ICC across two cortical regions (i.e. motor vs. sensory) within two different time intervals (blocks vs. days). We found sensory regions had higher MUA firing rate stability than motor regions (Fig 5B, left; $F_{(1, 30)} = 21.6; p < 0.001$) and shorter times intervals (i.e. minutes) had higher MUA firing rate stability than longer time intervals (i.e. days) (Fig 5C, left: $F_{(1, 30)} = 4.4; p = 0.045$). However, there was no a significant interaction between cortical region and time interval ($F_{(1, 30)} = 2.71; p = 0.11$). The results indicate

that the consistency between the mean firing rate of a specific channel was greater for sensory than motor channels and greater shorter than longer periods of time.

MUA shape is not affected by passage of time

We compared the mean MUA shape of active channels along a timescale of minutes (i.e. blocks) and days. In contrast to MUA firing rates, we observed that waveforms in active channels maintained similar shapes and amplitudes across minutes and sessions (Fig. 4B and 4D). Using a two-way repeated measures ANOVA to compare the ICC across two cortical regions (i.e. motor vs. sensory) within two different time intervals (blocks vs. days) for each channel, we found a significant effect for cortical area (Fig 5B, right: $F_{(1,152)} = 9.68, p < 0.005$) where MUA shape within sensory channels was more consistent than within motor channels. However, we did not observe an effect for time interval (Fig 5C, right: $F_{(1,152)} = 0.22, p = 0.64$) nor an interaction between cortical area and the time intervals ($F_{(1,152)} = 0.72; p = 0.40$). Altogether, this suggests that, MUA shape over time within electrodes was more consistent within sensory channels than within motor channels, but was robust to passage of time.

DISCUSSION

Nearly all channels implanted in the hand knob were active for multiple muscle group regions in a representative motor array - including facial and distal leg regions, controlled and paralyzed muscles, as well as contralateral and ipsilateral sides – despite occupying laterally opposite somatotopic regions and encompassing representations both above and below the level of injury. In addition, we found significant differences in both spatial stability and MUA firing patterns (mean firing rate and PTSH shape) across timescales on the order of minutes and days. Importantly, as the timescale of comparison increased, the dissimilarity in both the spatial and MUA patterning dynamics increased. Notably this variance was higher in motor MEAs as compared to sensory MEAs.

Characterizing the whole-body sensorimotor map

Isolated-muscle group contractions in our study participant were associated with multiunit-level neural representations of both intact and paralyzed muscles that were diffuse and overlapping, with a typical channel coding for multiple muscles distributed throughout both sides of the body. Altogether, the map provides evidence of a global and bilateral body somatosensory representation within the hand knob and somatosensory cortex. This is particularly noteworthy, as this violates the longstanding notion of S1 somatotopy in which neighboring regions of the body are represented in adjacent cortical areas, in favor of a fractionated somatotopy similar to M1. Our findings align with another study that characterized the somatotopy of entire limb movements within the hand knob of M1 and found whole-body tuning (Willett et al., 2020). However, in contrast to the somatotopy found by Willet et al, our spatial patterning appeared far more fractionated and mosaic. This difference in fractionation could be because our methods relied on a much more stringent muscle-specific task, controlling for any concurrent extraneous or postural activity, whereas Willett et al. focused on micromovements that likely engage multiple muscle groups simultaneously. Moreover, our criterion for neural activation was based on the presence of a statistically significant modulation with respect to baseline, whereas they classified active channels based on the ability of the PSTH to discriminate between movements, regardless of whether each separate micromovements each generated statistically significant responses.

Motor multi-unit activity is relatively unstable after days and even minutes

Importantly, to date, we are the first to systematically characterize both the somatotopic and MUA firing response stability for activating the same muscle within the same individual across multiple timepoints. We found highly variable spatial and firing pattern stability across motor arrays not only over the course of days, but even minutes.

On the order of minutes, the somatotopy and firing patterns at the MUA-level in both motor cortices is only moderately consistent (Fig. 4C,D). Across days, this consistency breaks down to the extent that only a tiny minority of motor channels were consistently active across all 8 days (Fig. 4A, B), which in turn suggests that muscle-related encoding in our motor cortex recordings was highly unstable.

Sensory channels are more consistent than motor channels, in spatial distribution and average response firing rate

In contrast to motor areas, the spatial pattern and temporal shape of units in both sensory cortices was fairly consistent across both minutes and days, (Fig. 4C, D). Indeed, the majority of sensory channels were consistently active across all 8 days, whereas most active motor channels tend to be active only for occasional sessions. Likewise, the similarity of the multiunit response over time tends to be fairly consistent whether the interval between comparisons is on the order of minutes or days; in contrast, motor channel response time courses have low correlations across days.

Overall, the spatial arrangement and MUA firing patterns in motor cortex tended to be more sporadic across days, whereas somatosensory cortex often retained similar somatotopy and firing patterns. The fact that our participant is capable of fully executing wrist extensions raises the possibility that much of the sensory response that we observe is due to feedback from these movements. While this is almost certainly a factor, further analysis of our data suggests that the picture is more nuanced, as we also observed sensory activity during contraction attempts of paralytic muscles (including the ring and little fingers).

Implications on decoding for brain-machine interfaces (BMIs)

The durability of a given decoder mapping for a BMI depends implicitly on the long- and short-term stability of MUA activity patterns. Our findings suggest that decoders that weight neural activity based on the activities of specific channels during a training period may have limited longevity because the underlying neural code, especially in the motor cortex, modifies over short timescales. While this feature may be biologically beneficial (i.e. the brain encodes descending muscle commands in a robust manner through redundancy), it may also complicate the inference of the current design of neural decoders (i.e. a particular combination of neural activity generated by a muscle contraction at one instance of time means that the same combination of neural activity will continue to be recruited for future iterations of this contraction). Rather, a better

long-term strategy may be to account for a more thorough description of neural activity embodied in the overall dynamics of the response across channels. Recent advances in decoding algorithms, that consider not only whole-trial dynamics, but activity patterns at a higher level of abstraction than individual electrodes (Gallego et al., 2017, Schroeder et al. 2019, Degenhart et al. 2020) offer a promising solution and may expand the repertoire of BMI-controllable tasks by providing greater robustness over time. Furthermore, the existence of possible efference copy signals in our sensory recordings, together with our observation that they are more stable over time (in terms of average firing rate increases) suggest that decoder stability may be improved by sampling from the somatosensory cortex.

FUNDING:

This research was developed with funding from the Defense Advanced Research Projects Agency's (DARPA, Arlington) Revolutionizing Prosthetics program (contract number N66001-10-C-4056). The views, opinions, and/or findings expressed are those of the author(s) and should not be interpreted as representing the official views or policies of the Department of Defense or the U.S. Government. Development of experimental setup and support for regulatory submissions associated with this study were provided by a grant from the Alfred E. Mann Foundation. Study software infrastructure and study preparation were developed with internal funding from Johns Hopkins University Applied Physics Laboratory and the Johns Hopkins School of Medicine.

ACKNOWLEDGEMENTS:

We thank the participant for their enthusiastic participation; this participant was also involved in the studies described in submissions MEDRXIV/2020/117374 and MEDRXIV/2020/116913. We gratefully acknowledge Drs. Kendra Cherry-Allen, Jennifer Keller, and Ed Connor for helpful discussion and consultation. This study was conducted under Investigational Device Exemption (IDE, 170010) by the Food and Drug Administration (FDA) for the purpose of evaluating bilateral sensory and motor

capabilities of microelectrode array implants in people affected by tetraplegia. It is registered on clinicaltrials.gov as NCT03161067.

REFERENCES

Ajiboye AB, Willett FR, Young DR, Memberg WD, Murphy BA, Miller JP, Walter BL, Sweet JA, Hoyen HA, Keith MV, Peckham PH, Simeral JD, Donoghue JP, Hochberg LR, Kirsch RF (2017). "Restoration of Reaching and Grasping Movements through Brain-Controlled Muscle Stimulation in a Person with Tetraplegia: A Proof-of-Concept Demonstration." *The Lancet* 389 (10081): 1821–30. https://doi.org/10.1016/S0140-6736(17)30601-3.

Becker RF (1953). The Cerebral Cortex of Man. By Wilder Penfield and Theodore Rasmussen. The Macmillan Company, New York, N.Y. 1950. 248 Pp." *American Journal of Physical Anthropology* 11 (3): 441–44. https://doi.org/10.1002/ajpa.1330110318.

Birn RM, Molloy EK, Patria R, Parker T, Meier TB, Kirk GR, Nair VA, Meyerand ME, Prabhakaran V (2013). The effect of scan length on the reliability of resting-state fMRI connectivity estimates. *Neuroimage*, 83, 550-558, 2013. https://doi.org/10.1016/j.neuroimage.2013.05.099

Bouton CE, Shaikhouni A, Annetta NV, Bockbrader MA, Friedenberg DA, Nielson DM, Sharma G, Sederberg PB, Glenn BC, Mysiw WJ, Morgan AG, Deogaonkar M, Rezai AR (2016). Restoring Cortical Control of Functional Movement in a Human with Quadriplegia. *Nature* 533 (7602): 247–50. https://doi.org/10.1038/nature17435.

Carmena JM, Lebedev MA, Henriquez CS, Nicolelis MAL (2005). Stable Ensemble Performance with Single-Neuron Variability during Reaching Movements in Primates. *Journal of Neuroscience* 25 (46): 10712–16. https://doi.org/10.1523/JNEUROSCI.2772-05.2005.

Chestek CA, Batista AP, Santhanam G, Yu BM, Afshar A, Cunningham JP, Gilja V, Ryu SI, Churchland MM, Shenoy KV (2007). Single-Neuron Stability during Repeated Reaching in Macaque Premotor Cortex. *Journal of Neuroscience* (40): 10742–50, 2007. https://doi.org/10.1523/JNEUROSCI.0959-07.2007.

Churchward PR, Butler EG, Finkelstein DI, Aumann, TD, Sudbury A, Horne, MK (1997). A comparison of methods used to detect changes in neuronal discharge patterns. *Journal of neuroscience methods*, 76(2), pp.203-210. https://doi.org/10.1016/S0165-0270(97)00099-X

Collinger JL , Wodlinger B, Downey JE, Wang W, Tyler-Kabara EC, Weber DJ, McMorland AJC, Velliste M, Boninger ML, Schwartz AB (2013). High-Performance Neuroprosthetic Control by an Individual with Tetraplegia. *The Lancet* 381 (9866): 557–64. https://doi.org/10.1016/S0140-6736(12)61816-9.

Degenhart AD, Bishop WE, Oby,ER, Tyler-Kabara EC, Chase SM, Batista AP, Yu BM (2020). Stabilization of a brain–computer interface via the alignment of low-dimensional spaces of neural activity. *Nat Biomed Eng,* 1-14. https://doi.org/10.1038/s41551-020-0542-9

De Luca C, Gilmore LD, Kuznetsov M, Roy SH (2010). Filtering the surface EMG signal: Movement artifact and baseline noise contamination. *Journal of biomechanics* 43 (8), 1573-1579. https://doi.org/10.1016/j.jbiomech.2010.01.027

Downey JE, Schwed N, Chase SM, Schwartz AB, Collinger JL (2018). Intracortical recording stability in human brain—computer interface users. Journal of neural engineering 5(4), 46016, https://doi.org/10.1088/1741-2552/aab7a0

Eifuku, S., De Souza, W.C., Tamura, R., Nishijo, H. and Ono, T., 2004. Neuronal correlates of face identification in the monkey anterior temporal cortical areas. *Journal of neurophysiology*, *91*(1), pp.358-371. https://doi.org/10.1152/jn.00198.2003

Franchi G. (2002) Time Course of Motor Cortex Reorganization Following Botulinum Toxin Injection into the Vibrissal Pad of the Adult Rat. *European Journal of Neuroscience* 16 (7): 1333–48. https://doi.org/10.1046/j.1460-9568.2002.02195.x.

Fraser GW, Schwartz AB (2012). Recording from the Same Neurons Chronically in Motor Cortex." *Journal of Neurophysiology* 107 (7): 1970–78. https://doi.org/10.1152/jn.01012.2010.

Gallego JA, Perich MG, Miller LE, Solla SA (2017). Neural Manifolds for the Control of Movement."*Neuron* 94 (5): 978–84. https://doi.org/10.1016/j.neuron.2017.05.025.

Ganguly K, Carmena JM (2009). Emergence of a Stable Cortical Map for Neuroprosthetic Control. *PLoS Biology* 7 (7): e1000153. https://doi.org/10.1371/journal.pbio.1000153.

Gaser C, Schlaug G (2003). Brain Structures Differ between Musicians and Non-Musicians. *Journal of Neuroscience* 23 (27): 9240–45. https://doi.org/10.1523/JNEUROSCI.23-27-09240.2003.

Graziano M (2006). The organization of behavioral repertoire in motor cortex. *Annu Rev Neurosci*, 29: 105-34. https://doi.org/10.1146/annurev.neuro.29.051605.112924

Greenberg PA, Wilson FAW (2004). Functional Stability of Dorsolateral Prefrontal Neurons. *Journal of Neurophysiology* 92 (2): 1042–55. https://doi.org/10.1152/jn.00062.2004.

Hochberg, LR., Bacher D, Jarosiewicz B, Masse NY, Simeral JD, Vogel J, Haddadin S, Liu J, Cash SS, van der Smagt P, Donoghue JP (2012). Reach and Grasp by People with Tetraplegia Using a Neurally Controlled Robotic Arm. *Nature* 485 (7398): 372–75. https://doi.org/10.1038/nature11076.

Hochberg, LR, Serruya MD, Friehs GM, Mukand JA, Saleh M, Caplan AH, Branner A, Chen D, Penn RD, and Donoghue JP (2006). Neuronal Ensemble Control of Prosthetic

Devices by a Human with Tetraplegia. *Nature* 442 (7099): 164–71. https://doi.org/10.1038/nature04970.

Klaes C , Kellis S, Aflalo T, Lee B, Pejsa K, Shanfield K, Hayes-Jackson S, Aisen M, Heck C, Liu C, Andersen RA (2015). Hand Shape Representations in the Human Posterior Parietal Cortex. *Journal of Neuroscience* 35 (46): 15466–76. https://doi.org/10.1523/JNEUROSCI.2747-15.2015.

Klaes C, Shi Y, Kellis S, Minxha J, Revechkis B, Andersen RA (2014). A Cognitive Neuroprosthetic That Uses Cortical Stimulation for Somatosensory Feedback. *Journal of Neural Engineering* 11 (5): 056024. https://doi.org/10.1088/1741-2560/11/5/056024.

Kleim JA, Barbay S, Nudo RJ (1998). Functional Reorganization of the Rat Motor Cortex Following Motor Skill Learning. *Journal of Neurophysiology* 80 (6): 3321–25. https://doi.org/10.1152/jn.1998.80.6.3321.

Levakova M, Tamborrino M, Ditlevsen S, Lansky P (2015). A review of the methods for neuronal response latency estimation. BioSystems 136, 23-34. https://doi.org/10.1016/j.biosystems.2015.04.008

Leyton ASF, Sherrington CS (1917). Observations on the excitable cortex of the chimpanzee, orangutan, and gorilla. *Quarterly Journal of Experimental Physiology* 11 (2): 135–222. https://doi.org/10.1113/expphysiol.1917.sp000240.

Li CS, Padoa-Schioppa C, Bizzi E (2001). Neuronal Correlates of Motor Performance and Motor Learning in the Primary Motor Cortex of Monkeys Adapting to an External Force Field. *Neuron* 30 (2): 593–607. https://doi.org/10.1016/s0896-6273(01)00301-4.

Lotze M, Erb M, Flor H, Huelsmann E, Godde B, Grodd W (2000). FMRI Evaluation of Somatotopic Representation in Human Primary Motor Cortex. *NeuroImage* 11 (5 Pt 1): 473–81. https://doi.org/10.1006/nimg.2000.0556.

Maunsell JH, Gibson JR (1992). Visual response latencies in striate cortex of the macaque monkey. *Journal of Neurophysiology*, 68(4), pp.1332-1344. https://doi.org/10.1152/jn.1992.68.4.1332

Meier, JD, Aflalo TN, Kastner S, Graziano MSA (2008). Complex Organization of Human Primary Motor Cortex: A High-Resolution FMRI Study. *Journal of Neurophysiology* 100 (4): 1800–1812. https://doi.org/10.1152/jn.90531.2008.

Nudo RJ., Milliken GW. 1996. Reorganization of Movement Representations in Primary Motor Cortex Following Focal Ischemic Infarcts in Adult Squirrel Monkeys. *Journal of Neurophysiology* 75 (5): 2144–49. https://doi.org/10.1152/jn.1996.75.5.2144.

Nudo RJ, Milliken GW, Jenkins WM, Merzenich MM (1996). Use-Dependent Alterations of Movement Representations in Primary Motor Cortex of Adult Squirrel Monkeys. *Journal of Neuroscience* 16 (2): 785–807. https://doi.org/10.1523/JNEUROSCI.16-02-00785.1996

Nudo RJ, Wise BM, SiFuentes F, Milliken GW (1996). Neural Substrates for the Effects of Rehabilitative Training on Motor Recovery after Ischemic Infarct. *Science* 272 (5269): 1791–94. https://doi.org/10.1126/science.272.5269.1791.

Penfield W, Boldrey E (1937). Somatic motor and sensory representation in the cerebral cortex of man as studied by electrical stimulation. *Brain* 60 (4): 389–443. https://doi.org/10.1093/brain/60.4.389.

Rokni U, Richardson AG, Bizzi E, Seung HS (2007). Motor Learning with Unstable Neural Representations. *Neuron* 54 (4): 653–66. https://doi.org/10.1016/j.neuron.2007.04.030.

Schieber, MH, Hibbard LS (1993). How somatotopic is the motor cortex hand area? *Science*, 261 (5120), pp.489-492. https://doi.org/10.1126/science.8332915

Schieber MH , Lang CE, Reilly KT, McNulty P, Sirigu A (2009). Selective Activation of Human Finger Muscles after Stroke or Amputation. In *Progress in Motor Control* (pp. 559–75). Springer, Boston, MA. https://doi.org/10.1007/978-0-387-77064-2_30.

Schroeder KE, Perkins SM, Wang Q, Churchland MM. Neural control of virtual ego-motion enabled by an opportunistic decoding strategy. bioRxiv. https://doi.org/10.1101/2019.12.13.862532

Shrout PE,Fleiss JL (1979). Intraclass correlations: uses in assessing rater reliability. *Psychological bulletin*, *86*(2), 420-428. https://doi.org/10.1037/0033-2909.86.2.420

Sugase-Miyamoto Y, Richmond BJ (2005). Neuronal signals in the monkey basolateral amygdala during reward schedules. *Journal of Neuroscience*, *25*(48), pp.11071-11083. https://doi.org/10.1523/JNEUROSCI.1796-05.2005

Suner S, Fellows MR, Vargas-Irwin C, Nakata GK, Donoghue JP (2005). Reliability of signals from a chronically implanted, silicon-based electrode array in non-human primate primary motor cortex. IEEE Trans Neural Syst Rehabil Eng 13(4), 524-541.doi: 10.1109/TNSRE.2005.857687

Willett FR, Deo DR, Avansino DT, Rezaii P, Hochberg L, Henderson JM, Shenoy K (2020). Hand Knob Area of Premotor Cortex Represents the Whole Body in Compositional Way. Cell 181, 1-14. https://doi.org/10.1016/j.cell.2020.02.043

FIGURES

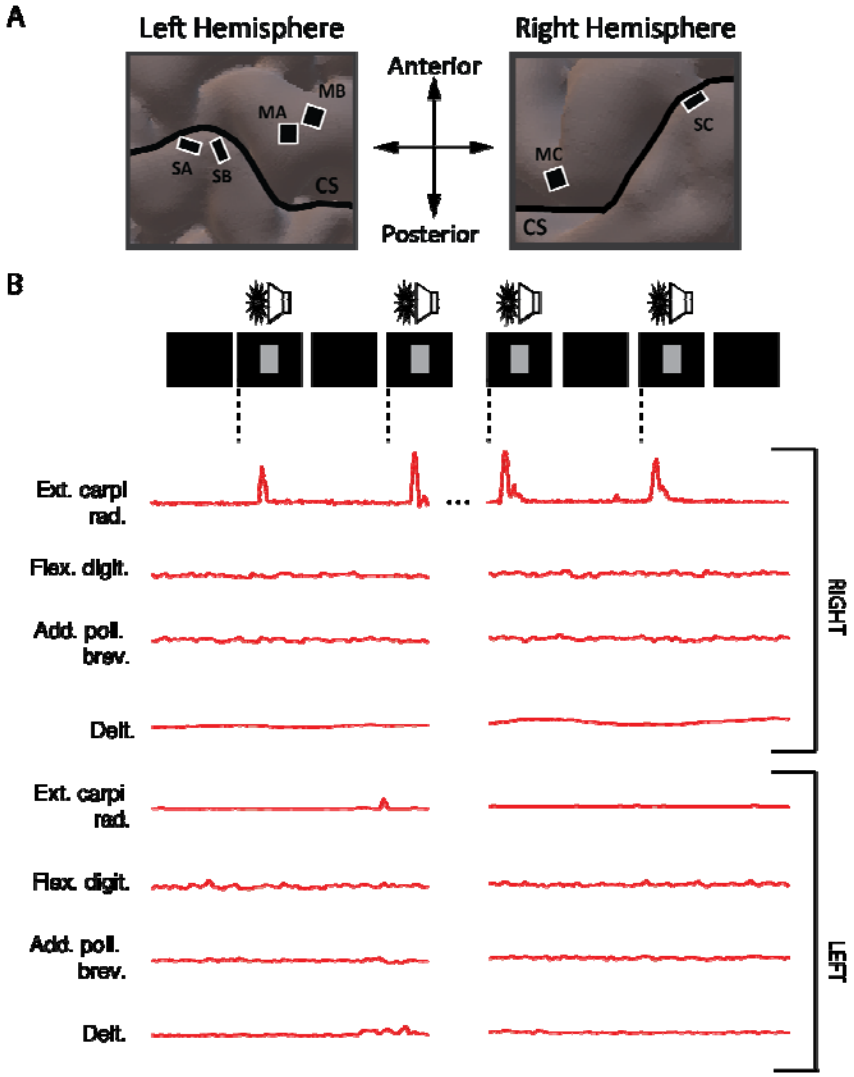

Figure 1: Cortical recording sites and experimental structure. A: Sites of the six bilaterally-implanted microelectrode arrays (MEAs), superimposed on MRI reconstruction of participant's brain (CS: central sulcus). Arrays are labeled by two-letter codes identifying the area of cortex and pedestal (e.g. MA: primary motor cortex, pedestal A; SB: primary sensory cortex, pedestal B). B: Overview of experimental paradigm. Each block was preceded by instructions specifying the isolated muscle group contraction to be performed, followed by a sequence of metronome ticks (combined auditory click and pixel flash) occurring at 4-second intervals. The cue signaled the participant to execute the movement when muscular control was intact (or

attempt the movement to the degree possible when control was impaired). Blocks consisted of 30 trials (i.e. metronome ticks). C: EMG traces for an example block of controlling the ECR.

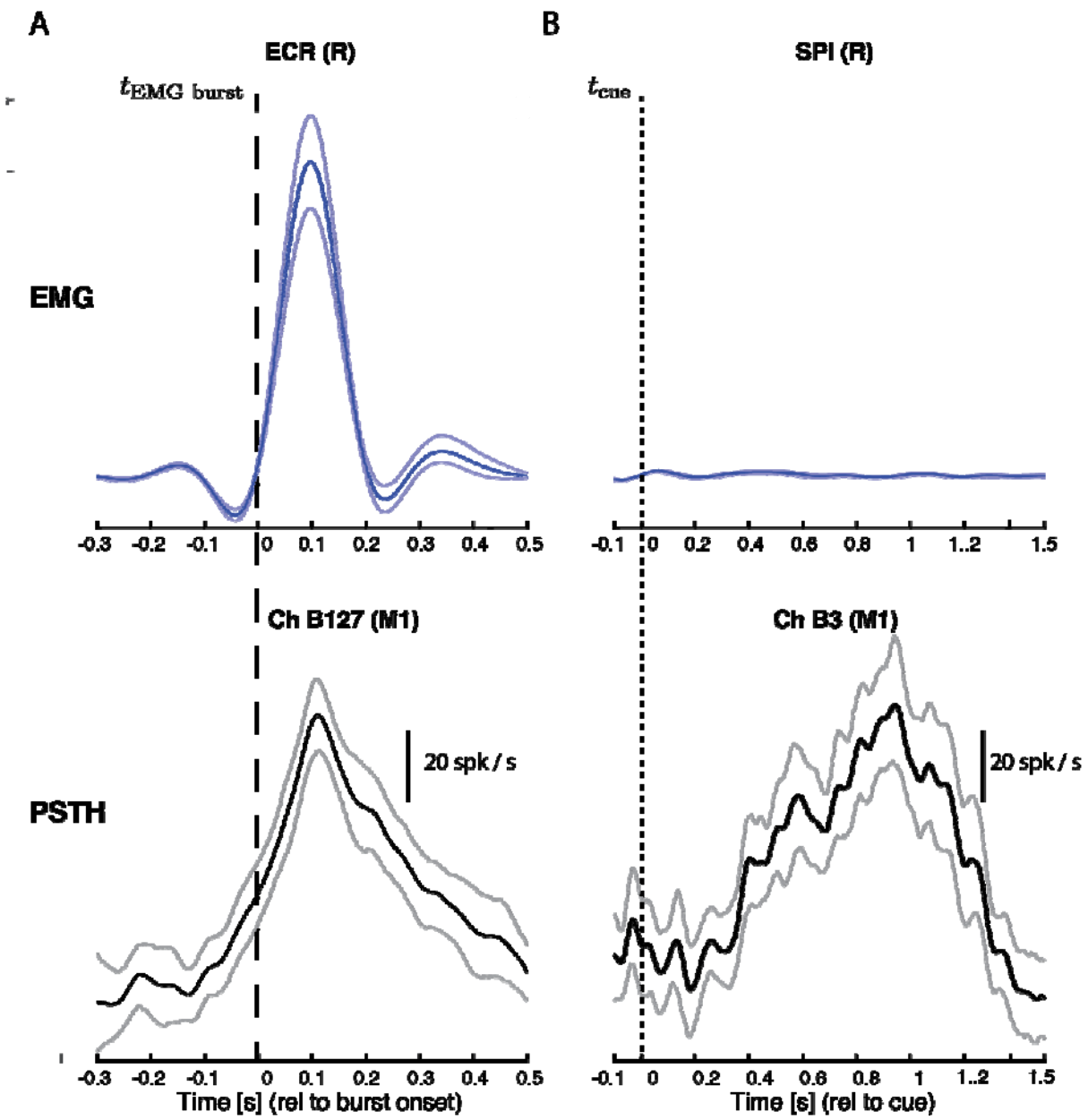

Figure 2: Temporal referencing for PSTHs. All data is plotted as the mean across 30 trials for a representative EMG recording (top panels) or PSTH of a given channel (bottom panels), with bootstrapped 95%--confidence interval (shaded region). X-axis from EMG panels denotes time relative to EMG onset (vertical dashed line) and y-axis signifies EMG amplitude. X-axis for PSTH denotes time relative to cue onset (vertical dashed line) and y-axis represents mean firing rate in spikes/second. A: For muscles with retained function (ECR: extensor carpi radialis, right side), the onset of the EMG burst (top panel) was detected with a sliding--window approach (dashed line; see

Methods for details), and multi-unit activity for any channel (bottom) was analyzed with respect to the burst onset time. B: For paralytic muscles with no EMG bursting (SPI: 2nd palmar interosseus, right side), all activity was referenced to the onset of the metronome cue and analyzed over an extended window to accommodate the response delay. EMG traces and multiunit activity are drawn on identical scales.

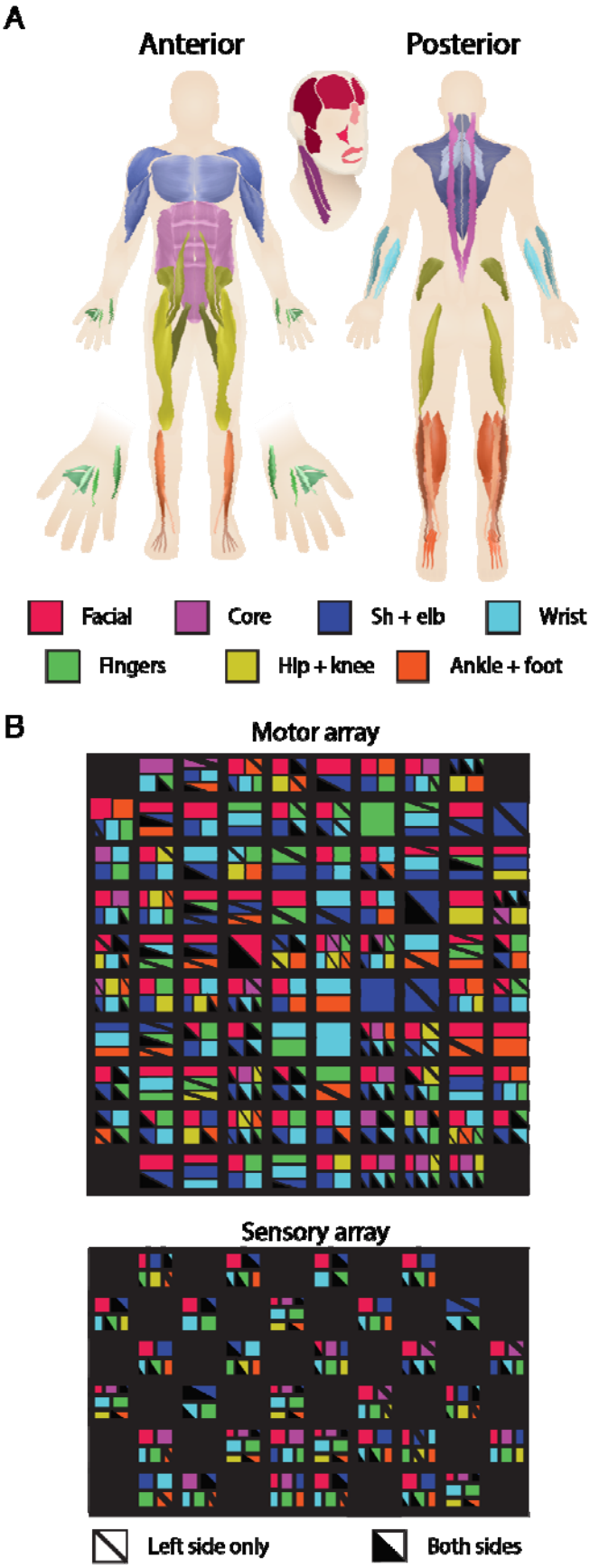

Figure 3: Full-body sensorimotor motor map characterization. A: Overview of assessed isolated-muscle group contractions, color-coded by body region. B: Top panel - topography of motor MEA in the left hemisphere (pedestal B), bottom panel – topography of sensory MEA in the left hemisphere (pedestal B). Channels with significant MUA associated with an isolated group muscle contraction color coded by body region and laterality. Solid colors denote contralateral activity (i.e. from right side of the body), a diagonal line denotes ipsilateral activity (i.e. from left side of the body), and a black solid triangle denotes bilateral activity (i.e. from both sides of the body).

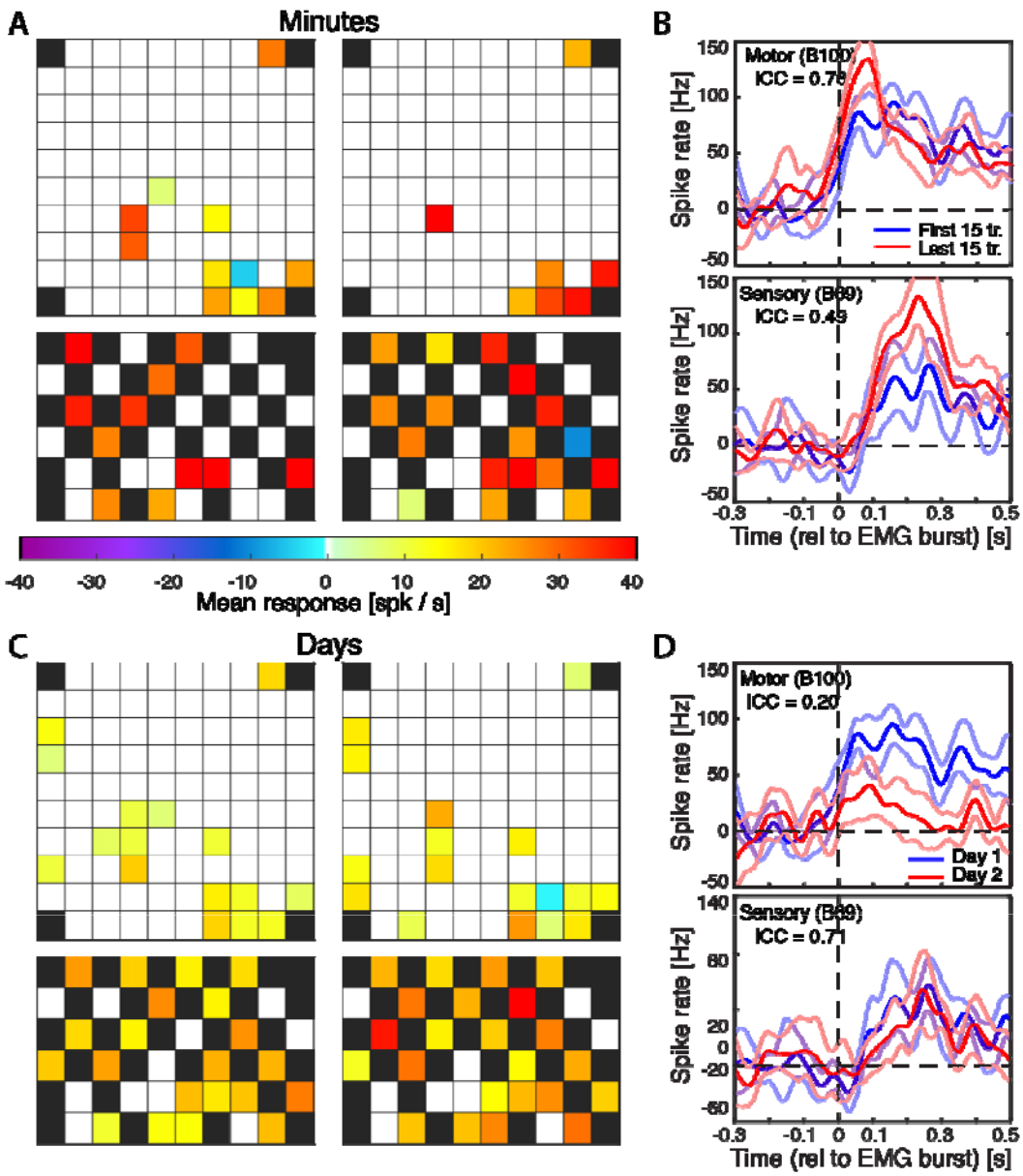

Figure 4: Stability of cortical activity during muscle contractions of the right ECR. A: Channel activations of motor (top row) and sensory (bottom) MEAs on pedestal B over consecutive blocks (i.e. within minutes) relative to baseline. Each cell represents an electrode location, corresponding to a distinct patch of cortex. Activity is the trial-averaged mean firing rate for each channel with warmer colors denoting higher firing rates, with baseline subtracted (spikes/second). B: PSTHs of a representative motor (top) and sensory (bottom) channel. The x-axis denotes time relative to EMG burst onset (as marked with a vertical dashed line). Blue and red traces are trial-averaged

PSTHs across the first 15 and second 15 trials within a block, respectively. Shaded regions represent bootstrapped 95%-confidence intervals about the mean. Intraclass correlation (ICC) is reported as a measure of similarity between waveforms. C: Channel activations of motor (top row) and sensory (bottom) MEAs over a span of days. D: Comparison of PSTHs for a representative motor (top) and sensory (bottom) channel across days.

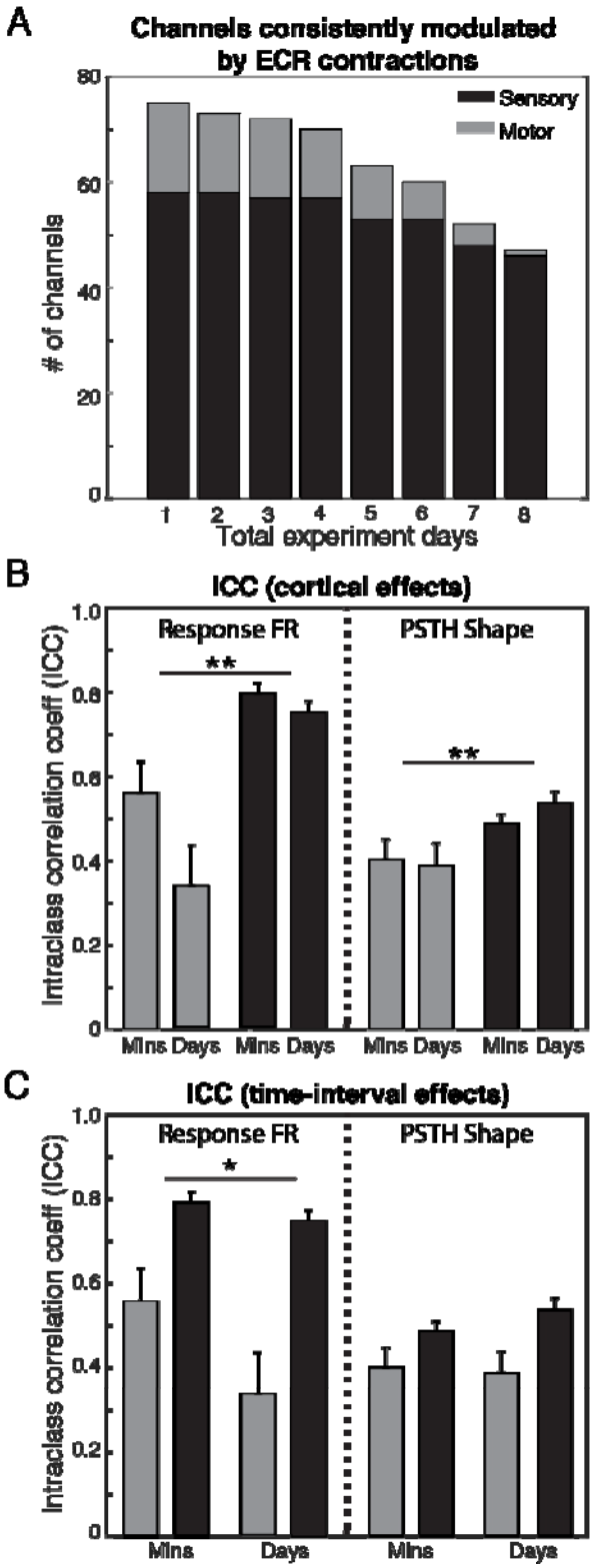

Figure 5: Consistency of multiunit responses within motor and sensory cortices for ECR sensorimotor map. A: Number of channels (y-axis) responding to muscle activations for each subset of experiment days (x-axis) for motor (gray) and sensory (black) channels. B: Distribution of Intraclass Correlation Coefficients (ICCs) for mean firing rates (FR) during response periods (left sector), and whole-PSTH shape (right) for motor and sensory cortices are grouped by brain region (x-axis). Significant main effects of brain region were noted for mean response FR and for PSTH shape. Data are means ± SEM. Asterisks (**) denote significant main effects of cortical region ($p < 0.01$). C: Distribution of ICCs for response FR and PSTH waveform shape (y-axis) grouped by timescale (x-axis). Data are means ± SEM. Asterisks (*) denote a significant main effect of cortical region on response FR ($p < 0.05$)